The interaction of multiferroic properties and interfaces in hexagonal $LuMnO_3$ ceramics

A Baghizadeh[1], J M Vieira[1], D G Stroppa[2], P Mirzadeh Vaghefi[3], M P Graça[4], J S Amaral[3], M-G.Willinger[5] and V S Amaral[3]

[1]*Department of Materials & Ceramic Engineering & CICECO, Aveiro University, 3810-193 Aveiro, Portugal*
[2]*Quantitative Electron Microscopy Group, International Iberian Nanotechnology Laboratory, 4715-330 Braga, Portugal*
[3]*Physics Department & CICECO, Aveiro University, 3810-193 Aveiro, Portugal*
[4]*Physics Department & I3N, Aveiro University, 3810-193 Aveiro, Portugal*
[5]*Department of Inorganic Chemistry, Fritz Haber Institute of the Max Planck Society, Faradayweg 4-6, 14195 Berlin, Germany*
Email: ali.baghizhadeh@ua.pt

A study on the underlying interaction mechanisms between lattice constants, magnetic and dielectric properties with inhomogeneities or internal interfaces in hexagonal, off-stoichiometric $LuMnO_3$ oxide is presented. By increasing Mn content the a-axis constant and volume of the unit cell, the antiferromagnetic (AFM) Néel temperature, T_N, and frustration factor of the frustrated Mn^{3+} trimmers in basal plane show decreasing trends. It was found that increasing annealing time improves properties of the lattices and progressively eliminates secondary phases for compositions within the solid solution stability limits. A magnetic contribution below T_N is observed for all samples. Two regimes of magnetization below and above 45 K were observed in the AFM state. The magnetic contribution below T_N is assigned to either secondary phase or internal interfaces like ferroelectric (FE) domain walls. Magneto-dielectric coupling at T_N is preserved in off-stoichiometric ceramics. The presence of a low temperature anomaly of the dielectric constant is correlated to composition of the solid solution in off-stoichiometric ceramics. Large FE domains are observed in PFM images of doped and un-doped ceramics, whereas atomic structure analysis indicates parallel formation of nano-sized FE domains. Combination of measured properties and microscopy images of micron- and nano-sized domains ascertain the role of lattice distortion and stability of solid solution on multiferroic properties.

Keywords: multiferroics, $LuMnO_3$, microscopy, interfaces, ferroelectrics

Introduction

Multiferroic materials are actively investigated because different properties co-exist together providing feasibility for the study of mutual interaction of the lattice, magnetization and ferroelectricity [1]. One of the most demanding family among multiferroics is h-$RMnO_3$ oxides where coupling of magnetic ordering to electrical polarization and lattice was reported [2,3]. In ceramics of h-$RMnO_3$ oxides stoichiometry shifts, sintering temperature and time, grain boundaries and interfaces were showed to influence the properties of the lattice [4–8]. Perhaps that is why in different reports scattered values or different behavior were obtained in the investigated properties. Both magnetic and dielectric properties present anomalies at the AFM transition temperature T_N as an intrinsic property of the lattice. Additional anomalies in magnetic or dielectric behavior were reported in h-$RMnO_3$ oxides where contributions of secondary phases or spin canting as a result of unit cell distortion or interfaces in the lattice were discussed [4,9–12]. Interlocking of FE walls to structural domain walls with subsequent distortion of the lattice was given as a driving force for appearing intriguing properties like net magnetization or fascinating cloverleaf topology of FE domain networks [13–15]. Therefore, it looks necessary to pursue with detailed studies the contribution of chemical inhomogeneities and internal interfaces (nano-scale features) on multiferroic properties of bulk ceramics.

In this article, self-doping in h-$LuMn_xO_{3\pm\delta}$ ($0.92 \leq x=Mn/Lu \leq 1.12$) ceramics was chosen to introduce chemistry shifts in the lattice, by creating either Mn-excess or Lu-excess in lattice of the solid solution. The effects of stoichiometry shifts on unit cell parameters, magnetic and dielectric properties and ferroelectric domains are studied. Annealing time is used to control residuals of secondary phases, the extent of internal interfaces or chemical inhomogeneities of the lattices. Modification of

the measured properties is correlated to the different annealing time which results in further understanding of the interaction of cation vacancies, properties and sintering condition. Beyond of bulk properties, microstructural investigation was performed by means of microscopy techniques like aberration corrected and non-corrected STEM in combination to EELS and EDS spectroscopies to identify the nano-scale phenomena in the lattices of the ceramics. Microscopy analysis assists us to explain some of the anomalies observed in the measured bulk properties driven by chemistry shift or interfaces or both.

Methods

The $LuMn_xO_{3\pm\delta}$ ($0.92\leq x=Mn/Lu\leq 1.12$) ceramics prepared by mixing due amounts of raw oxides, MnO_2 and Lu_2O_3, were sintered in three steps by changing the time and temperature of annealing [12]. The last step of high temperature holding was done at 1300 °C for one day, 5 days or 10 days. XRD measurements were done for all sintered ceramics using Philips XPERT XRD Diffractometer with Cu Kα source, in the range of $10°\leq 2\theta\leq 100°$ with 0.013° step. Rietveld refinement of the XRD patterns were performed using Fullprof Suit 3 to create the structural file of each ceramic [16]. Magnetic measurements were done by using QUANTUM Design SQUID MPMS3 both in AC and DC modes. The null measurement was performed on the brass holder to acquire the background magnetic signal in the absence of samples. The field-cooled (FC) and zero-field cooled (ZFC) measurements were all done under 100 Oe applied field from 350 K down to 5 K. The scanned field in field dependent magnetization measurements ranged from -5.5 T to 5.5 T. The first derivative of magnetic data versus temperature was used to calculate the T_N of each composition. The values of T_{CW} were calculated after subtracting the amount of hausmannite (Mn_3O_4) secondary phase extracted from XRD Rietveld refinement and resulted in ±50 K error in final reported values [12]. Dielectric measurements were performed using LCR meter with frequency range from 100 Hz to 1 MHz in a closed-cycle cryostat cooler allowing cooling of the sample down to 10 K. Precision Impedance Analyzer Agilant 429A was used for ac measurements.

NT-MDT NTEGRA AURA modular sensor force microscope was used for AFM/PFM measurements at room temperature in contact mode with 10 V AC voltage and 50 kHz frequency on the tip. Cantilevers from NanoSensor Co., Pointprobe-Plus Silicon-SPM-Sensor made of n^+-doped silicon coated by Al on the detector side with 10 nm tip radius were used for all measurements. The mechanical polishing for either PFM or TEM analysis was used down to 0.5 micron or 0.1 micron diamond grits. Final finishing for TEM/STEM analysis was completed using gentle ion milling. The 200 kV Hitachi HD2700 dedicated STEM equipped with both EDS and secondary electron detectors was used for STEM/EDS characterization. EELS spectra of the regions of the interest in HRTEM were acquired in the Philips CM200 FEG TEM equipped with a GIF Quantum energy filter and Tridiem camera. HAADF-STEM images of sub-Angstrom resolution were taken in the Cs/probe-corrected Titan Themis TEM/STEM microscope operated at 300 kV, 30 mrad convergence angle and over 80 mrad collection angle for HAADF detector.

Results and discussion

Figure 1(a) shows the change of a-constant of crystalline lattice cell with Mn/Lu ratio (x) for each annealing time in h-$LuMn_xO_{3\pm\delta}$ in the whole composition range ($0.92\leq x=Mn/Lu\leq 1.12$) of this study. Both a-constant and volume of the unit cell follow trendy behavior from left side to right side of the solid solution stability range. The effect of annealing time is mainly decreasing the fluctuation of the results determined in samples upon increasing the annealing time to 5 and then 10 days in comparison to those of samples annealed in a short time. Additionally, the limit of the solid solution stability comes out of the longer annealing cycles, 5 days, sets the upper limit at x=1.04, whereas 10 days defines the lower limit at x=0.96. In either annealing time the shrinking of a-constant is observed from low x to high x sides. Figure 1(b) and (c) give the variation of the Néel transition temperature of basal plane AFM interaction among Mn^{3+} ions and Curie-Weiss temperature T_{CW}, respectively [17]. The overall trend for T_N is a decreasing with increasing values of x (from 88 K to 94 K). Like lattice constants, annealing time makes the observed dependences of T_N and T_{CW} on sample composition

smoother. Inside the stability bounds of the h-$LuMn_xO_{3\pm\delta}$ solid solution T_{CW} increases in a regular way with x. T_{CW} values of x<1 samples range from -1100 K to -700 K. On the x>1 side T_{CW} increases up to -550 K in samples with total Mn excess above the upper stability limit of the solid solution. Curie-Weiss temperature of x<1 shows larger sensitivity to the sintering time, values of T_{CW} decreased as time of annealing is extended.

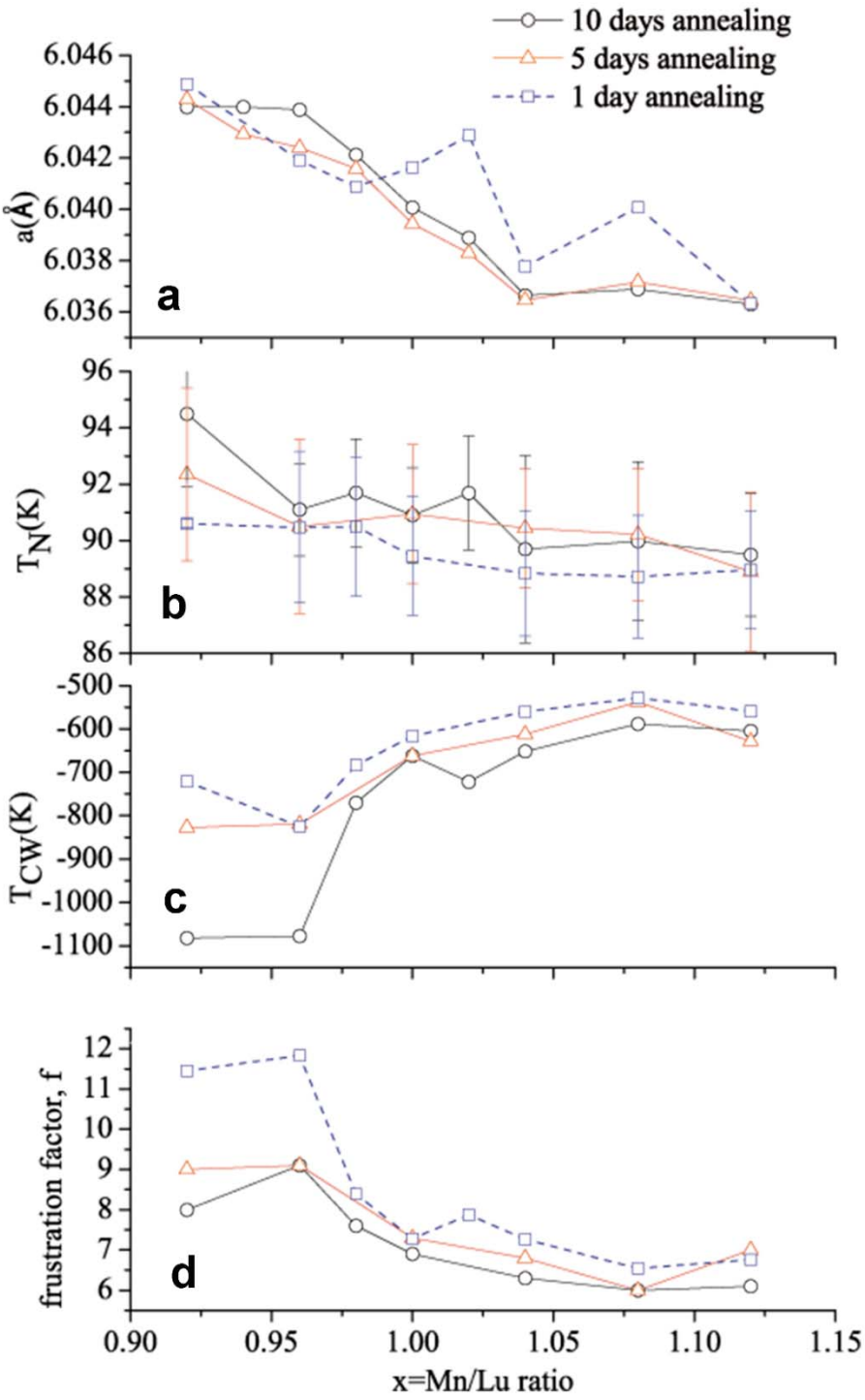

Figure 1. (a) Values of a-axis constant of the crystalline cell versus x at three different values of annealing time. (b) T_N values and (c) T_{CW} versus x, (d) frustration factor, f, as the ratio of absolute values of T_{CW} to T_N. In all measured properties the increase in annealing time reduces fluctuation on reported values.

Comparison is made to the dependence of T_{CW} of $YMn_xO_{3\pm\delta}$ on x from two independent studies with bulk ceramic samples, for x≤1 [6] and x≥1 [18]. In the low x≤1 side, the effect of Mn/Y ratio on the values of T_{CW} is opposite to the one observed in $LuMn_xO_{3\pm\delta}$ in the present study. In the Mn-rich side of $YMn_xO_{3\pm\delta}$ the values of T_{CW} also decrease until x reaches the threshold of x=1.08 the trend being reversed above this value. Data of T_{CW} of $YMn_xO_{3\pm\delta}$ converged to similar values as seen in Figure 1(c) for samples $LuMn_xO_{3\pm\delta}$ with x>1.04. Calculated from T_N values and T_{CW} values in Figure1(b) and (c) the frustration factor $f = |T_{CW}/T_N|$ [19] in Figure1(d) gives an indication of the diminished frustration of the Mn trimers in basal plane of the hexagonal lattice as composition moves from the high Lu-excess side to the high Mn-excess side. Frustration factor f covers a wide range of values from 11.5 for x=0.92 to 5.6 for x=1.08 (Figure 1(d)). Magnetic frustration has been discussed as driven by the titling of the MnO_5 bipyramids and buckling of the Lu planes inside the crystalline cell [19–21]. Both T_{CW} and f demonstrate the important role of type of vacancies in the cation sublattices and their concentrations in self-doping of h-$RMnO_3$ lattices. For $LuMnO_3$ of nominally stoichiometric composition values of T_{CW} and f in the present study stay between -700 K and -600 K and between 7 and 8, respectively. Values of f and T_{CW} of $LuMnO_3$ polycrystals of nominally stoichiometric composition were reported as 5.8 (T_{CW} = -519 K) [22], 6.76 (T_{CW} = -602 K) [23], 8.25 (T_{CW} = -750 K) [21] and for $LuMnO_3$ single crystal 10.3 (T_{CW} = -887 K) [17]. The measured values of these magnetic parameters of the polycrystalline ceramics in current study fit well the range of values of $LuMnO_3$ materials of same composition reported in literature.

In the rare study of the effect of annealing temperature on properties of the h-$RMnO_3$ phases, $YMnO_3$ polycrystalline samples were prepared by sintering for short period of 4 hours in oxygen atmosphere at different annealing temperatures from 900 °C to 1400 °C [24]. The increasing of annealing temperatures yielded the phase transition from orthorhombic phase (SG Pnma) to hexagonal phase (SG $P6_3cm$) at 900 ºC, faster grain growth, improved final density and changed crystalline unit cell parameters as well as magnetic properties and dielectric permittivity. In the same study, $YMnO_3$ samples display AFM ordering and T_{CW} becomes negative only for sintering temperatures above 1100 °C, the values of T_{CW} decreasing to more negative values as the temperature of annealing was further increased. The present study on the effect of annealing time on the magnetic properties of sintered h-$LuMn_xO_{3\pm\delta}$ materials reveals that at 1300 ºC the sintering time above 24 hours actually is barely effective on changing the main trends of T_{CW} and f.

The modification of lattice parameters seen in Figure 1(a) may in part explain the observed change of T_{CW} and f parameter in Figure 1(c) and Figure 1(d). Upon 5 days annealing, volume and a-axis of the crystalline cell of x>1 samples converged to nearly equilibrium values and the observed trend is not modified by further increasing annealing time to 10 days. However, the opposite side of composition samples with x<1 showed some instability in measured values of the lattice parameters even for the longest annealing time. T_{CW} and f are linked to tilting of the MnO_5 polyhedral and buckling in planes of the unit cell. By increasing the ionic radius from Sc to Lu and then from Lu to Y in h-$RMnO_3$ oxides, the tilting of MnO_5 polyhedral and buckling of R planes decrease as also decrease in parallel T_N and $|T_{CW}|$ [19, 23]. The a-axis constant and volume of the unit cell both indicate expansion by increasing ionic radius of rare-earth ion, but the trend in c-constant is not monotonic. In the same way as h-$RMnO_3$ oxides with different R ions did show the dependency of the lattice parameters and magnetic parameters linked to the distortion in the unit cell, Figure 1(a), (b) and (c) of the current study also indicate that analogous effects of changes of the unit cell on magnetic properties can be created by self-doping.

Figure 2(a) presents the field-cooled (FC) and zero field-cooled (ZFC) magnetic susceptibility of three representative samples of x=0.96, x=1.00 and x=1.04 after 10 days annealing. For the set of samples of one day annealing it was found out upon cooling below T_N, FC magnetization increases at 43 K, more visible for samples of x>1 where traces of hausmannite secondary phase were found [12]. Increasing annealing time would expectedly reduce the contribution of hausmannite still the magnetic signal of the remains of the secondary phase is obvious in Figure 2(a). Among the selection of compositions in Figure 2(a), the sample with excess Mn contains higher amount of secondary phase, whereas magnetic signal below 43 K of the stoichiometric sample and the one with excess Lu has significantly dropped indicating a minor amount of the secondary phase. It should be noted that Bragg diffraction peaks corresponding to the hausmannite secondary phase in XRD patterns appear as very faint peaks, visible at $2\theta = 32.5°$ [12]. The irreversibility observed in FC vs ZFC magnetizations in

Figure 2(a) starts right at T_N and exists for all samples at different annealing conditions or compositions.

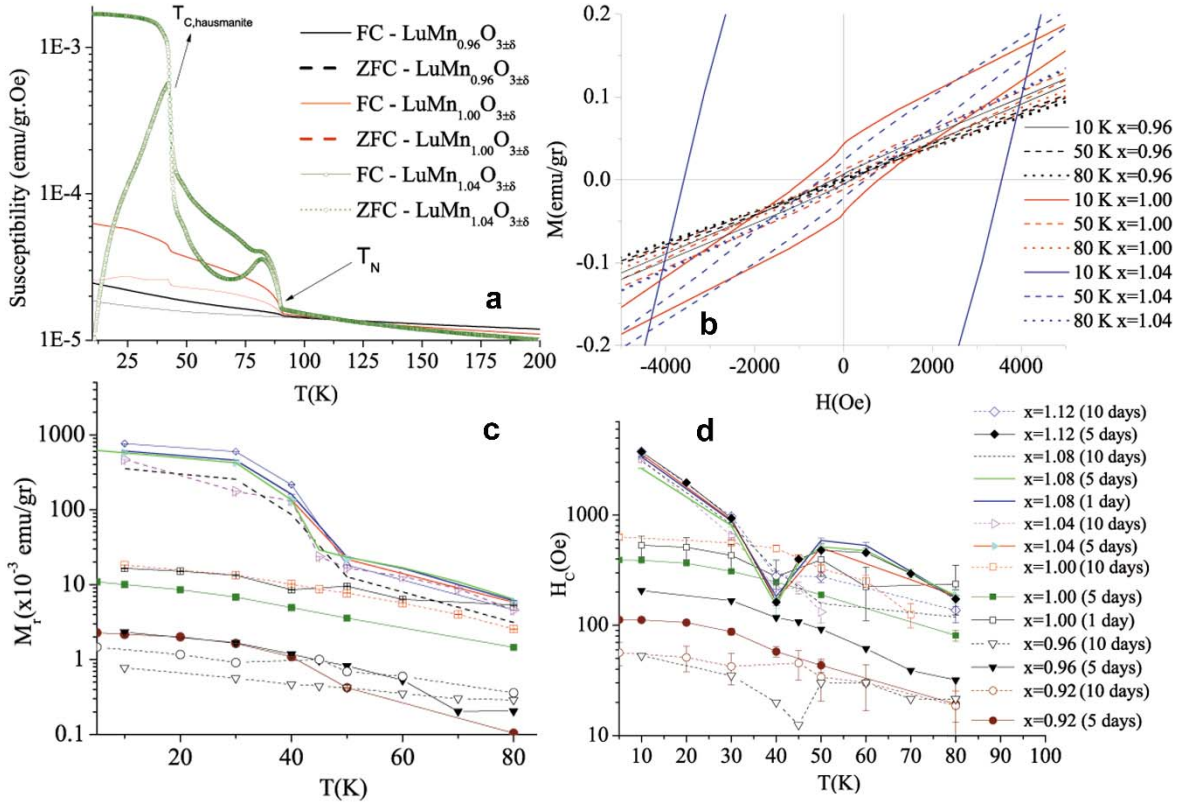

Figure 2. (a) FC vs. ZFC magnetic susceptibility for three selected compositions of 10 days annealing measured at 100 Oe external field, the AFM transition being marked as T_N. T_C holds for the ferrimagnetic Curie transition of hausmannite phase. (b) Field dependent magnetization of the same three samples taken at 10 K, 50 K and 80 K. For better reading of the details a narrow range of -0.5 T to 0.5 T is shown here. Magnetic remanence (c) and coercivity (d) of selected samples reveal the presence of two magnetic components below T_N. The contribution of the secondary phase for samples of x>1 is clear from current magnetic measurements.

To further elucidate the irreversibility in magnetic susceptibility of sintered ceramics field dependent magnetization was determined below T_N on selected samples of each annealing condition. Comparison is done in Figure 2(b) for samples of same three compositions of Figure 2(a) at fixed temperatures of 10 K, 50 K slightly above Curie temperature T_C of hausmannite and 80 K, just below T_N of the main phase, Figure 1(b). The main features to retain here are the slope of the M-H curves when they enter the linear parts at high fields above 1 T associated to the AFM behavior of the material and the opening of the M-H loops revealing the additional magnetic component besides the AFM one. The effect of the second magnetic component is visible below 43 K modifying the hysteresis of magnetization versus field cycles of sample x=1.04. The difference in the M-H curves below and above 43 K is less visible in samples with x≤1. It is expected that most of the revealed hysteresis in magnetic loops above 43 K must come from the main phase either originated in the crystalline lattice or from internal interfaces.

The presence of net magnetization in current ceramics sets two different temperature regions below T_N in Figure 2(a) and (b). To further clarify the origin of magnetization in these two regions the magnetic remanence and coercivity below T_N were determined for samples of all compositions of this study. Figure 2(c) shows the remanence, M_r, from 5 K to 80 K for samples with different annealing conditions. Samples in this figure can be divided into two sets according to their behavior. In one set, samples of x>1 have a large decreasing in M_r between 40 K and 50 K. It closely replicates the analogous decrease of FC magnetization under 100 Oe applied field in the same range of temperatures in Figure 2(a). As mentioned earlier, this knee in M_r must be assigned to the Mn_3O_4 secondary phase or else to planes with intergrowths of Mn-O phases. In the second set, those samples with x≤1 show a

rather regular decrease of M_r with T with just a slight bending of M_r when crossing the same range of temperatures. Above T_C of hausmannite the values of M_r of samples with x>1 become of the same order of magnitude as the M_r of the samples with nominally stoichiometric composition (x=1.00). The M-H hysteresis cycles revealed exchange bias effects in the magnetic behavior in 5-80 K temperature range of samples of all compositions of this study. Coercive field, H_c, in Figure 2(d) was calculated as $H_c = |H_+ - H_-|/2$ where H_+ and H_- are the coercivity fields on increasing field and decreasing field branches of the M-H loop, respectively [7,9]. Almost the same division in two groups of samples is observed concerning the dependence of the H_c on T, as it was found for the M_r. The values H_c as a function of T in Figure 2(d) reveal the presence of a drop in H_c in the temperature range of 40 – 45 K for samples with x>1. While by analogy with the values of M_r for compositions with x>1 one would expect to observe a decreasing trend of H_c as temperature rises from T_C of Mn_3O_4 and approaches the value of T_N of the main phase, in fact the values of H_c of some of these samples rise again at temperatures above 50 K and latter converge to the values of coercive field H_c determined in the samples with nominally stoichiometric composition (x=1.00).

Ceramics sintered with the short annealing time of one day showed the change in dielectric constant around T_N which confirmed the magneto-dielectric coupling in the whole solid solution range of h-$LuMn_xO_{3\pm\delta}$ ceramics [12]. Presence of some anomalies in dielectric constant below T_N was attributed to inhomogeneity of the samples of short annealing time. Temperature dependent complex dielectric constant was measured for selected samples after 5 days annealing in order to study the effect of longer annealing time. Figure 3(a) gives the real part of the dielectric constant, ε′, as a function of T in the range 10-200 K, for representative samples with x=0.92, x=1.00 and x=1.04. All three samples clearly show the transition of the dielectric constant coupled to AFM ordering at temperatures labelled as T^*_N very close to the values of T_N of the magnetic measurements in Figure.1(b). As in Figure 3(a), a second transition below 90 K is also seen here, being more prominent for the x=0.92 sample with the maximum of dε′/dT at 75 K, Figure 3(b), but still noticed in the x=1.04 sample as an ill-defined broad transition in the temperature range 70-78 K in Figure 3(a). This second transition of the dielectric permittivity has no correspondence with any transition that could be detected in magnetic susceptibility measurements of the same samples. Although the same transition was observed in stoichiometric samples of short annealing time it vanished and is no longer detected after 5 days annealing. The symmetrical appearance of this second transition below T_N in the x=0.92 and x=1.04 samples suggests the potential effect of vacancy doping on the dielectric behavior of the crystalline lattice which may provoke bond distortion or perhaps creates regions (nanodomains or interfaces) of inhomogeneity in the crystalline structure. The determination of ε* with different frequencies confirmed that the anomaly of ε′associated to T_N and the second transition of the same property observed below T_N in the samples in Figure 3(a) are athermal. As previously reported in samples of 1 day annealing, an anomaly in ε′ is observed at temperatures below 35 K for the x=0.92 sample in Figure.3(b) which is frequency dependent and thermally activated [12]. The corresponding Arrhenius plot of the relaxation time as a function of inverse of temperature at the local maximum of ε′′ for frequencies above 10 KHz in Figure 3(c) is linear. The same analysis of data from the x=1.00 and x=1.04 samples did not display any visible peak in this temperature range, neither in real nor in the imaginary parts of permittivity. The fitting of the Arrhenius plot to the experimental data in Figure 3(c) yields 18.6 meV for the activation energy, close to the corresponding value of 12 meV obtained for the relaxation time of ε′′ for x=1.08 Mn-rich sample of one day annealed [12].

The lacking of the second transition below T_N in x=1.00 sample and of the low temperature peak in permittivity in x=1.00 and x=1.04 samples may carry relevant information. From Rietveld refinement of XRD data, the evolution of lattice parameters of samples with 1 day and 5 days annealing in Figure 1(a) show large differences. Not just is the scatter in data of the longer annealing time lesser, but also the lattice parameters a-axis and unit cell volume come to a sort of stability (linear plateau) for x≥1.04. This value can be set as the upper stability limit of the h-$LuMn_xO_{3\pm\delta}$ solid solution [12]. But the same could not be found for x<1 side with 5 days of annealing time. Only by duplicating the annealing time to 10 days, the equivalent plateau appeared for x<0.96 (Figure 1(a)) meaning that the Mn vacancy doped branch of the solid solution requires even longer annealing time to approach equilibrium and get properly ordered crystalline lattices. Within the limits of such inference the analysis of the dielectric constant would suggest that in Lu vacancy doped samples, a less disturbed

crystalline lattice showed up with vanishing of the thermally activated peak of ε′′ below 35 K and fading away of the second transition below T_N for x=1.04. These two peaks would be essentially extrinsic and hence absent in high quality single crystals. Ordering of ions in the crystalline structure of x=1 samples would be facilitated by the equal proportion of the Lu and Mn ions, the two extra transitions of ε′′ lacking in the corresponding results in Figure 3(a).

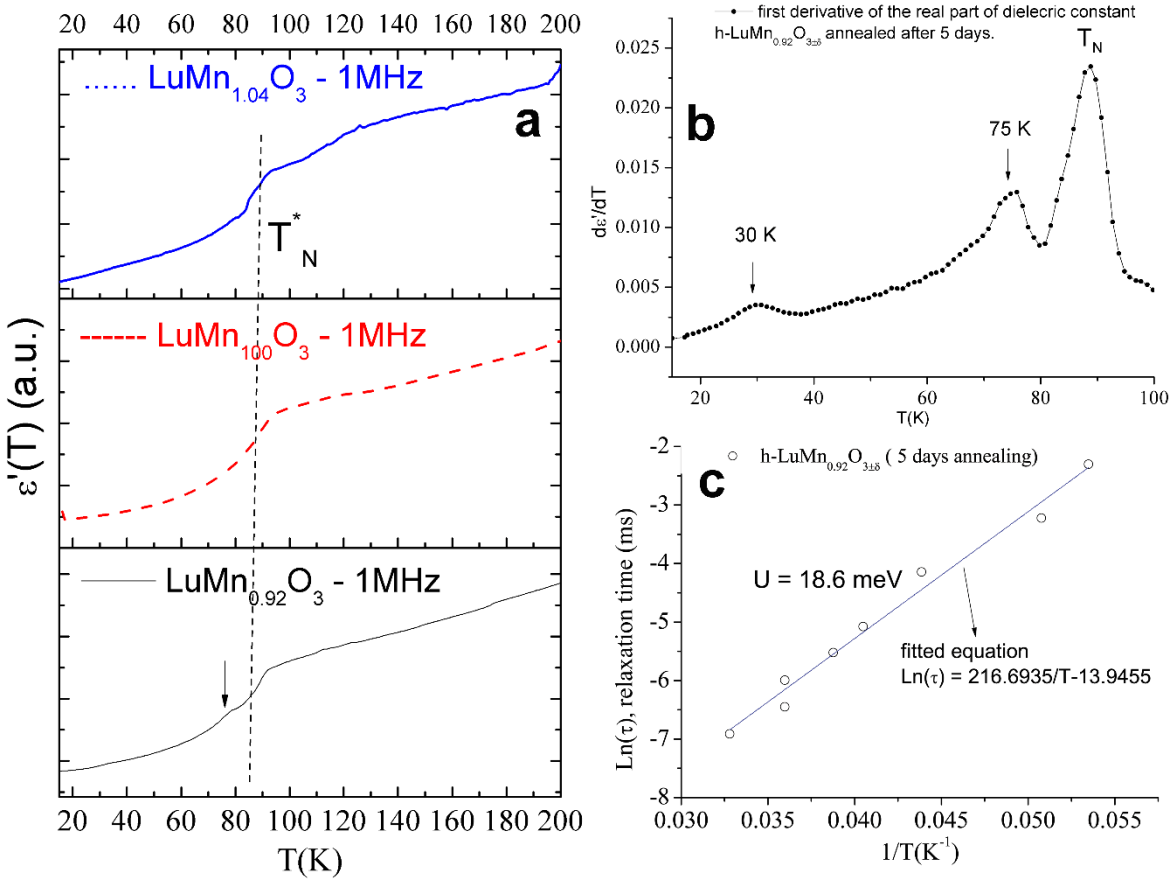

Figure 3. (a) Temperature dependent dielectric constant ε′(T) at 1 MHz frequency of three selected compositions from samples annealed for 5 days, the dash line gives approximate magnetic ordering transition. The abrupt change in ε′(T) here is labelled as T^*_N close to T_N of magnetic measurements. (b) Derivative of dielectric constant for the sample x=0.92 taken at 1 MHz showing 3 peaks, one at T_N (around 92 K) and others at 75 K and 30 K. (c) The anomaly of the imaginary permittivity of sample x=0.92 observed in 18 K to 30 K temperature range and frequencies above 10 KHz fits to the Arrhenius equation yields 18.6 eV of activation energy.

To shed light into anomalies observed in magnetic and dielectric measurements below T_N, comprehensive microscopy analysis was done on selected compositions of the different annealing conditions. Figure 4(a)-inset shows the SEM/EDS analysis of a x=1.12 sample annealed for one day taken at 200 keV with the secondary electron detector of the STEM microscope. The SEM image shows the interface between hausmannite and main phase. The EDS line profile in Figure 4(a) displays the change in Mn and Lu concentration across the line marked in Figure 4(a). The transition from the secondary phase to the main phase is as wide as 100 nm. The ratio of Mn/Lu does not show constant values inside the main phase until half a micron distance away of the interface is reached. This often observed widening of the interface region between the two phases, visible in samples of x>1, mostly at x=1.12, reveals formation of an intermediary region where concentration of Mn does not match its atomic percentage with either hausmannite or h-$LuMn_xO_{3\pm\delta}$ phase. Such an intermediary layer although in the order of few hundred nanometer wide, has the potential to modify the magnetic behaviour of the either phases. The microscopy analysis in support to the magnetic anomalies around

43 K leads to the conclusion that the secondary phase hausmannite and its interface with the main phase can add a magnetization component below 43 K in an AFM state of the hexagonal phase.

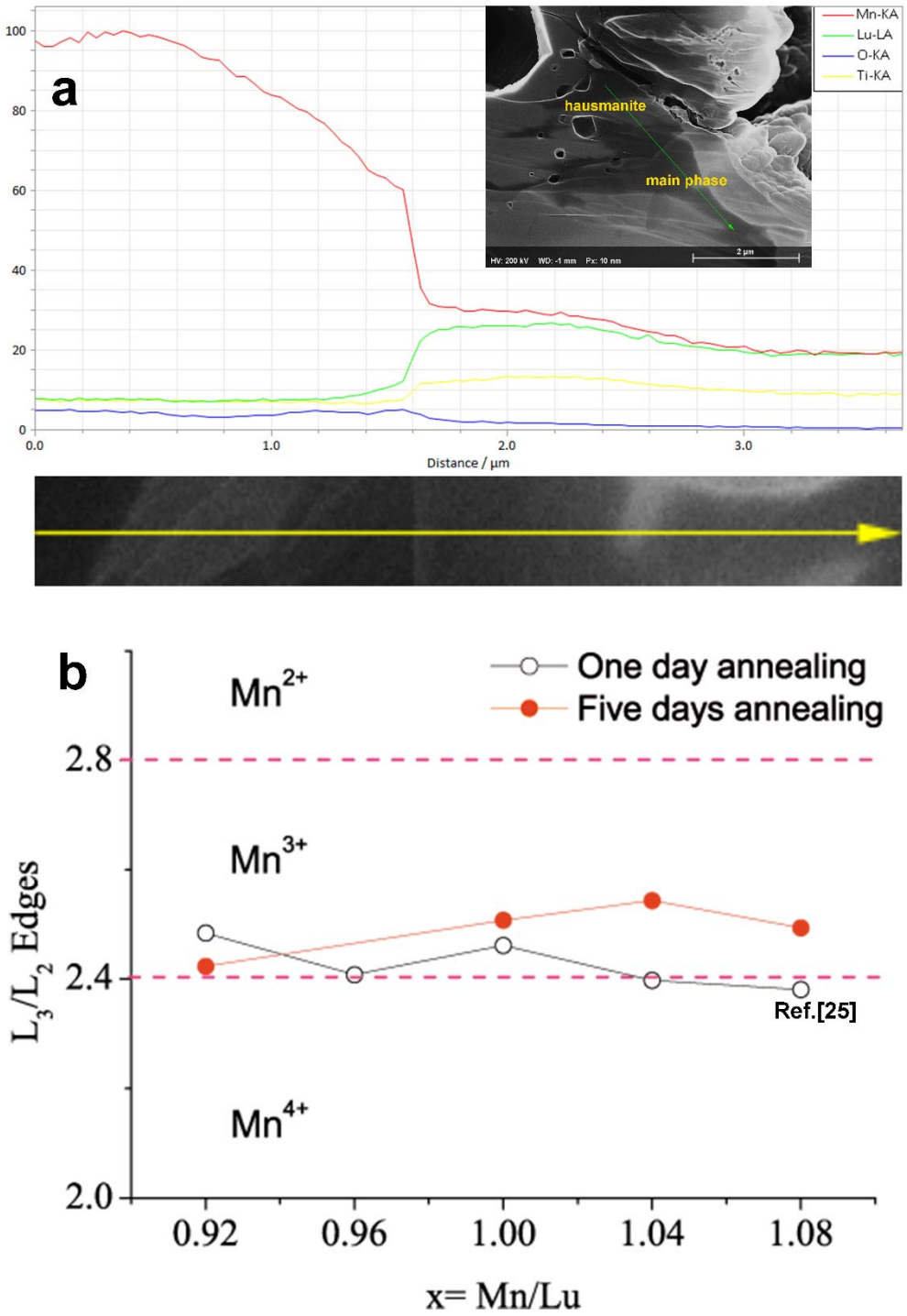

Figure 4(a) EDS-line profile of the interface of a hausmannite particle and main phase in sample h-$LuMn_{1.12}O_{3\pm\delta}$, 1 day annealing, showing the wide interface between two phases. Inset gives the SEM image (taken at 200 kV energy) of the region of analysis shown by the arrow. (b) The results of the white-line ratio analysis of the L_3 and L_2 peaks of the EELS spectra of the Mn ions taken in high magnification TEM indicate the rather constant oxidation state of the samples of 1 day [25] and 5 days annealing time which lays inside the confidence region of the valence state of 3+.

Any possible trace of deviation from the 3+ oxidation state of Mn inside the particles of the main phase can be traced using EELS spectroscopy at high magnification of TEM. The ratio of L_3/L_2 edges

of Mn ion gives the Mn oxidation states, which can be quantified by the method so-called "white line" ratio described elsewhere [26, 27]. To determine the white-line ratio on the Mn $L_{3,2}$ edges, the multiple scattering contribution was subtracted using Digital Micrograph Suit 1.84.1282, then a 10 eV window was chosen as scaling window in the region immediately after L_2 peak to be used as Hartree-Slater cross section step function. The subtracted $L_{3,2}$ peaks from the extracted step function were both integrated in the same energy window [25]. The average of the L_3/L_2 ratio taken from two different regions of each sample for 5 different compositions of 1 day and 5 days annealed ceramics is plotted as a function of x in Figure 4(b). The results for the L_3/L_2 ratio of h-$LuMn_xO_{3\pm\delta}$ samples with 1 day annealing are from Figure S3(b) of ref. [25]. Although the nature of covalent bonding may result in slight changes of the valence state the present analysis in Figure 4(b) exhibits a rather constant value of the Mn^{3+} oxidation state for all measurements, or very close to it [26–29]. Because the EELS measurements were done in HRTEM mode, the region of analysis is restricted to few nano-meters of area with lattice imaging ensuring the regularity of atomic spacing and absence of atom clustering in each region under analysis.

Having hausmannite phase responsible for magnetic anomalies around 43 K and below, the measured magnetization above 43 K in Figure 2 cannot be explained with its origin on the secondary phase. As mentioned above, in h-$RMnO_3$ materials the interlocking of FE domain walls and anti-phase structural domain walls results in symmetry breaking on the domain. The symmetry breaking on the walls was shown to introduce net magnetization in an AFM state of the material below its T_N [10,13,14]. In the PFM analysis of the current ceramics large size FE domains were observed, as well as 6-fold topological vortices larger than few microns depending on the composition and annealing time. Ferroelectricity was thoroughly investigated on the sintered h-$LuMn_xO_{3\pm\delta}$ ceramics in the current work. Figure 5(a)-(c) gives the PFM images of three samples of composition x=0.92, x=1.04 and 1.08, respectively, after long annealing time. FE domains can be observed in all samples with polarization up (lighter colours) and down (darker colours). The size of FE domains is generally in the order of few microns, also there are dispersed FE domains of smaller sizes inside either polarized region. For instance, in Figure 5(a), aside of large FE domains with downwards polarization (dark, brown colour), small regions of the same polarization are observed which are scattered in the regions with opposite polarization (lighter colour).

Figure 5(d) presents the HAADF-STEM image of h-$LuMn_{1.04}O_{3\pm\delta}$ particle after 10 days annealing which was aligned along <110> zone axis to make observation of FE domain walls possible. In the large particle shown in Figure 5(d) one may expect an area of single polarization across the particle as PFM analysis suggests it. The probe-corrected microscope was used to determine polarization direction of the particle upon analysing different parts of the particle. By tracking the displacement of the Lu ions which are considered to induce electrical polarization, we identify several regions where switching of the polarization is observed [30]. In the image on the left, the phase shift appears as a change from α^- to γ^+ polarized domains, whereas the image on right of the same Figure 5(d) shows a phase shift from α^- to β^+ polarization by our analysis of Lu displacement [32]. The dashed line in this late image separates two regions of opposite polarization. According to Tian et al [33], this structure of domain wall (DW) which includes sections both perpendicular to polarization direction (transversal domain wall, TDW) and parallel to the polarization direction (longitudinal domain wall, LDW) corresponds to Type-C (TDW+LDW) domain wall. Switching of electrical polarization on DW is atomically sharp as seen in the STEM images of Figure 5(c), a common feature of FE walls in h-$RMnO_3$ oxides [30, 32, 33]. Two selected regions on both sides of black spot in Figure 5(d) present areas of opposite polarization which implies that the FE domains in this particle are less than 200 nm wide (direction of the arrows represent polarization orientation). Although in the evaluation of FE domains the topological 6-fold vortices were not found in this particle, the large density of the FE domain walls in a particle of less than 3 micron size demonstrates their potential role on modification of properties driven by the interfaces [13,14]. Beside of FE walls, we often captured stacking faults and anti-phase boundaries where the original symmetry of the crystalline lattice of the non-distorted regions is no longer preserved [25].

That FE walls are coupled to AFM walls in AFM state of the material was experimentally demonstrated on single crystals of h-$YMnO_3$ [2]. It was also discovered that AFM domain boundaries

can exist isolated without being pinned to FE walls [2]. Artyukhin et al [14] used Landau theory to develop terms to correlate inhomogeneous trimerization to strain and hence clamping of magnetism to the structural/ferroelectric domain walls [14], having shown that spin ordering of Mn^{3+} ions changes wherever they meet the structural distortion on FE walls. Additionally, he showed that on the contrary of atomically sharp FE/structural domain walls [32], the AFM domain wall can have widths of 40 Å or higher. The breaking of spin ordering of Mn^{3+} ions in the AFM state at structural walls results in net magnetization along c-axis [14]. Unveiling the cross-coupling of magnetism and ferroelectricity in h-$RMnO_3$ oxides was accomplished by Das et al [13] by using the First-principles approach to show that both electrical polarization and the magnetic component along c-axis are sensitive to the magnitude of the trimer distortion in K_3 zone boundary. Since trimer distortion is what actually happens on FE walls interlocked to structural antiphase boundaries, her theoretical results again confirm the inducing of a net magnetic moment along c-axis on the FE walls of h-$LuMnO_3$ [13]. Thus, it is expected that by tuning the density of FE walls one will be able to change the magnitude of the induced net magnetization of the material in the AFM state.

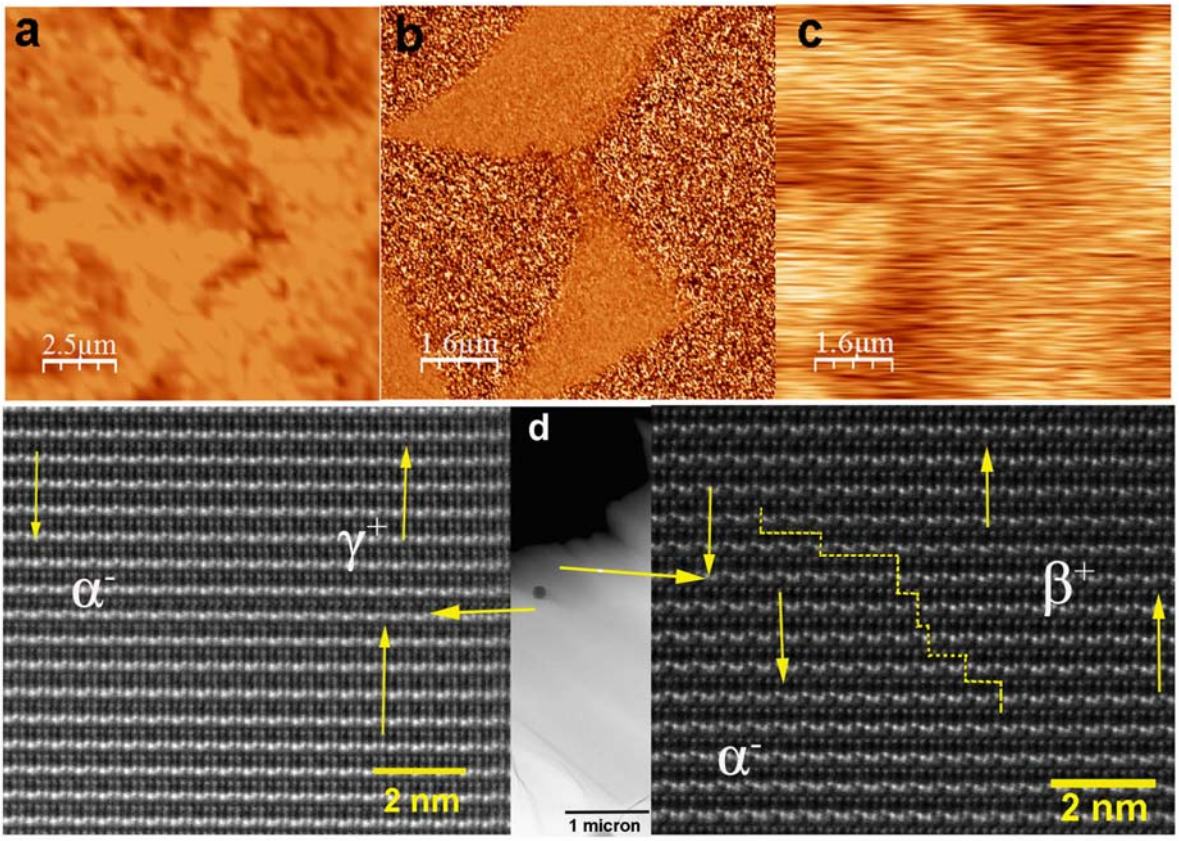

Figure 5 (a, b and c) PFM images of the self-doped ceramics of x=0.92 (a), x=1.04 (b) and x=1.08 (c) after 10 days annealing showing FE domains of 2 microns size or larger with up or down polarization. (d) HAADF-STEM image of a crystalline grain of sample x=1.04 (10 days annealing) aligned along <110> zone axis, the two images with atomic resolution on left and right sides of the figure were taken from the regions marked by the thick arrows. Thinner arrows in two images show the direction of polarization in correspondence with Lu displacements. The images show that several FE domains of different polarizations exist in a region of one micron wide. Phase shift of FE domains was determined as described in Ref.[32]. The dash line in STEM image (right picture) is a guide to eyes to show the position of Type-C FE wall.

Therefore, combination of accurate magnetic measurements in self-doped ceramics of the different compositions and electron microscopy/spectroscopy techniques revealed that the additional magnetic components below AFM ordering temperature of the Mn^{3+} spins most likely have two possible origins: First the magnetic transition around 43 K is attributed to magnetic transition of the hausmannite phase itself. Microscopy analysis of the interface of hausmannite and main phase provides a clear image of composition changes of Mn and Lu on the boundary of the two phases. This

interfacial region creates altered elemental ratio of Mn, Lu and O in a wide interfacial zone of tens nanometers, affecting magnetic properties around Curie temperature of hausmannite and below it [7,9]. However, the sole effect of the hausmannite phase and its related boundaries can be excluded in net magnetization detected above 45 K, as our magnetic measurements in Figure 2 show the same features for samples of $x \leq 1$. The second origin of net magnetization particularly above 45 K until T_N is assumed to mainly rise from disordering of the spins on the internal interfaces in grains of the main phase of the ceramics. Symmetry breaking on the FE walls where they are pinned to the structural domain walls theoretically resulted in spin rotation on the walls [14]. In general, the role of interfaces in h-$RMnO_3$ oxides has not yet been studied. Although most attention was devoted on exploring the properties of the 6-fold vortices in this family of multiferroic oxides, there are images of topology breaking of 6-fold vortices or structurally distorted cores [31–34]. The broad microscopy analysis of the FE domains in ceramics of the current study disclosed frequent topology breaking of the 6-fold vortices, also the interaction of the FE polarization and partial edge dislocations and stacking faults in the lattices, of which the effect on the magnetic properties requires more experiments and theoretical calculations via DFT approaches [25].

Conclusion

The present findings on lattice constants and magnetic parameters confirm that both composition and annealing time are affecting the properties of multiferroic h-$LuMn_xO_{3\pm\delta}$ materials in a trendy way. Lattice constants set a boundary on the stability limits of self-doped ceramics in the composition range of $0.96 \leq x \leq 1.04$, where traces of secondary phases of the Lu_2O_3 in the low x side and of Mn_3O_4 in the high side are visible. Hausmannite secondary phase detected either in measurement of magnetization and by electron microscopy suggests that the source of magnetic anomalies below 45 K reported in some other works is most likely this ferrimagnetic phase. Measured magnetic remanence between 45 K and T_N and observation of some anomalies in dielectric constant in this temperature range point to the contribution of the interfaces and extended defects which provoke local disordering of the lattice and spin canting. Ferroelectric domain observation showed the formation of large FE domains with dispersion of smaller FE domains. Atomic imaging of FE boundaries confirmed the high density of the FE walls in nano-scale and nano-FE domains of opposite polarization in sintered ceramics. Symmetry breaking at the FE walls and other planar defects captured in electron microscopy images is postulated to be the driving force for the additional magnetic component in AFM state of the current ceramics.

Acknowledgment

A. B. acknowledges the FCT fellowship SFRH/BPD/80663/2011 and Electron Microscopy Group in Fritz Haber Institute, Berlin for giving access to microscope for EELS analysis. A.B acknowledges Achim Klein-Hoffmann for assisting TEM sample preparation. We acknowledge the FCT project REDE/1509/RME/2005 in order to access all microscopes in pole of electron microscopy in Aveiro University. This work was developed within the scope of the project CICECO-Aveiro Institute of Materials, POCI-01-0145-FEDER-007679 (FCT Ref. UID /CTM /50011/2013), financed by national funds through the FCT/MEC and when appropriate co-financed by FEDER under the PT2020 Partnership Agreement

References

[1] Ramesh R and Spaldin N A 2007 Multiferroics: progress and prospects in thin films *Nat. Mater.* **6** 21–9

[2] Fiebig M, Lottermoser T, Frohlich D, Goltsev A V and Pisarev R V 2002 Observation of coupled magnetic and electric domains *Nature* **419** 818–20

[3] Lee S, Pirogov A, Kang M, Jang K-H, Yonemura M, Kamiyama T, Cheong S W, Gozzo F, Shin N, Kimura H, Noda Y and Park J G 2008 Giant magneto-elastic coupling in multiferroic hexagonal manganites *Nature* **451** 805–9

[4] Lorenz B 2013 Hexagonal Manganites—($RMnO_3$): Class (I) Multiferroics with Strong Coupling of Magnetism and Ferroelectricity *ISRN Condens. Matter Phys.* **2013** 43
[5] Chen W R, Zhang F C, Miao J, Xu B, Dong X L, Cao L X, Qiu X G, Zhao B R and Dai P C 2005 Re-entrant spin glass behavior in Mn-rich $YMnO_3$ *Appl. Phys. Lett.* **87** 42508
[6] Jeuvrey L, Pena O, Moure A and Moure C 2012 Synthesis and magnetic properties of hexagonal Y(Mn,Cu)O3 multiferroic materials *J. Magn. Magn. Mater.* **324** 717–22
[7] Belik A A 2014 Negative Exchange Bias in Polycrystalline Hexagonal ScMnO3 , InMnO3 , YMnO3 , 4H-SrMnO3 , and 6H -SrMnO3 and Perovskite YMnO3 : Effects of Impurities *J. Phys. Soc. Japan* **83** 74703
[8] Fedorova O M, Balakirev V F and Golikov Y V 2011 Composition Ranges of $Ln_{2-x}Mn_xO_{3+/-delta}$ (Ln = Y, Ho, Er) Solid Solutions between 900 and 1400°C in Air *Inorg. Mater.* **47** 192–5
[9] Kumar M, Choudhary R J and Phase D M 2015 Metastable magnetic state and exchange bias training effect in Mn-rich YMnO3 thin films *J. Phys. D. Appl. Phys.* **48** 125003
[10] Geng Y, Das H, Wysocki A L, Wang X, Cheong S-W, Mostovoy M, Fennie C J and Wu W 2014 Direct visualization of magnetoelectric domains. *Nat. Mater.* **13** 163–7
[11] Das R, Jaiswal A, Adyanthaya S and Poddar P 2010 Origin of Magnetic Anomalies below the Néel Temperature in Nanocrystalline $LuMnO_3$ *J. Phys. Chem. C* **114** 12104–9
[12] Baghizadeh A, Vieira J ., Amaral J S, Graça M P, Soares M R, Mota D A and Amaral V S 2015 Crystal structure, magnetic and dielectric behavior of h-$LuMn_xO_{3\pm\delta}$ ceramics ($0.95\leq x\leq 1.04$) *J. Magn. Magn. Mater.* **395** 303–11
[13] Das H, Wysocki A L, Geng Y, Wu W and Fennie C J 2014 Bulk magnetoelectricity in the hexagonal manganites and ferrites *Nat. Commun.* **5** 1–11
[14] Artyukhin S, Delaney K T, Spaldin N A and Mostovoy M 2014 Landau theory of topological defects in multiferroic hexagonal manganites *Nat. Mater.* **13** 42–9
[15] Kumagai Y and Spaldin N A 2013 Structural domain walls in polar hexagonal manganites *Nat. Commun.* **4** 1
[16] Rodriguez-carvajal J 1993 Recent advances in magnetic-structure determination by neutron powder diffraction *Phys. B* **192** 55–69
[17] Katsufuji T, Mori S, Masaki M, Moritomo Y, Yamamoto N and Takagi H 2001 Dielectric and magnetic anomalies and spin frustration in hexagonal $RMnO_3$ (R = Y, Yb, and Lu) *Phys. Rev. B* **64** 104419
[18] Chen W R, Zhang F C, Miao J, Xu B, Cao L X, Qiu X G and Zhao B R 2005 Magnetic properties of the self-doped yttrium manganites $YMn_{1+x}O_3$ *J. Physics-Condensed Matter* **17** 8029–36
[19] Katsufuji T, Masaki M, Machida A, Moritomo M, Kato K, Nishibori E, Takata M, Sakata M, Ohoyama K, Kitazawa K and Takagi H 2002 Crystal structure and magnetic properties of hexagonal $RMnO_3$ (R=Y, Lu, and Sc) and the effect of doping *Phys. Rev. B* **66** 134434
[20] Van Aken B B, Palstra T T M, Filippetti A and Spaldin N A 2004 The origin of ferroelectricity in magnetoelectric $YMnO_3$. *Nat. Mater.* **3** 164–70
[21] Park J G, Lee S, Kang M, Jang K-H H, Lee C, Streltsov S V., Mazurenko V V., Valentyuk M V., Medvedeva J E, Kamiyama T and Park J G 2010 Doping dependence of spin-lattice coupling and two-dimensional ordering in multiferroic hexagonal $Y_{1-x}Lu_xMnO_3$ ($0\leq x\leq 1$) *Phys. Rev. B - Condens. Matter Mater. Phys.* **82** 54428
[22] Tomuta D G, Ramakrishnan S, Nieuwenhuys G J and Mydosh1 J A 2001 The magnetic susceptibility, specific heat and dielectric constant of hexagonal $YMnO_3$, $LuMnO_3$ and $ScMnO_3$ *J. Phys. Condens. MATTER* **13** 4543–4552
[23] Uusi-Esko K, Malm J, Imamura N, Yamauchi H and Karppinen M 2008 Characterization of $RMnO_3$ (R=Sc, Y, Dy-Lu): High-pressure synthesized metastable perovskites and their hexagonal precursor phases *Mater. Chem. Phys.* **112** 1029–34
[24] Liu S-H, Huang J-C-A, Qi X, Lin W-J, Siao Y-J, Lin C-R, Chen J-M J M M, Tang M-T, Lee Y-H, Lee J-C J M M, Wu K H H, Gou I C C, Luo C W W, Uen T M M, Lin J-Y Y, Juang J Y Y, Chen C K K, Lee J-C 2011 Structural transformation and charge transfer induced ferroelectricity and magnetism in annealed $YMnO_3$ *AIP Adv.* **1** 32173
[25] Baghizadeh A, Vieira J M, Gonçalves J N, Willinger M G, Ferro M C and Amaral V S 2016 Nano-domains Coupled to FE Domains Induced by Lattice Distortion in Self-doped

$LuMn_xO_{3\pm\delta}$ Hexagonal Ceramics *J. Phys. Chem. C* acs.jpcc.6b04478
[26] Schmid H K and Mader W 2006 Oxidation states of Mn and Fe in various compound oxide systems. *Micron* **37** 426–32
[27] Riedl T, Gemming T and Wetzig K 2006 Extraction of EELS white-line intensities of manganese compounds: methods, accuracy, and valence sensitivity. *Ultramicroscopy* **106** 284–91
[28] Tan H, Verbeeck J, Abakumov A and Van Tendeloo G 2012 Oxidation state and chemical shift investigation in transition metal oxides by EELS *Ultramicroscopy* **116** 24–33
[29] Varela M, Oxley M P, Luo W, Tao J, Watanabe M, Lupini A R, Pantelides S T and Pennycook S J 2009 Atomic-resolution imaging of oxidation states in manganites *Phys. Rev. B* **79** 85117
[30] Zhang Q H, Wang L J, Wei X K, Yu R C, Gu L, Hirata A, Chen M W, Jin C Q, Yao Y, Wang Y G and Duan X F 2012 Direct observation of interlocked domain walls in hexagonal $RMnO_3$ (R = Tm, Lu) *Phys. Rev. B* **85** 020102(R)
[31] Wang X, Mostovoy M, Han M G, Horibe Y, Aoki T, Zhu Y and Cheong S-W W 2014 Unfolding of vortices into topological stripes in a multiferroic material *Phys. Rev. Lett.* **112** 1–5
[32] Zhang Q-H H, Tan G-T T, Gu L, Yao Y, Jin C-Q Q, Wang Y-G G, Duan X-F F and Yu R-C C 2014 Topology breaking of the vortex in multiferroic $Y_{0.67}Lu_{0.33}MnO_3$ *Appl. Phys. Lett.* **105** 12902
[33] Tian L, Wang Y, Ge B, Zhang X and Zhang Z 2015 Direct observation of interlocked domain walls and topological four-state vortex-like domain patterns in multiferroic $YMnO_3$ single crystal *Appl. Phys. Lett.* **106** 112903
[34] Li J, Chiang F-K, Chen Z, Ma C, Chu M-W, Chen C-H, Tian H, Yang H and Li J 2016 Homotopy-Theoretic Study & Atomic-Scale Observation of Vortex Domains in Hexagonal Manganites *Sci. Rep.* **6** 28047